

## MIT Open Access Articles

*Ultrasonic imaging front-end design for CMUT:  
A 3-level 30Vpp pulse-shaping pulser with  
improved efficiency and a noise-optimized receiver*

The MIT Faculty has made this article openly available. **Please share** how this access benefits you. Your story matters.

**Citation:** Chen, Kailiang, Anantha P. Chandrakasan, and Charles G. Sodini. "Ultrasonic Imaging Front-End Design for CMUT: A 3-Level 30Vpp Pulse-Shaping Pulser with Improved Efficiency and a Noise-Optimized Receiver." 2012 IEEE Asian Solid State Circuits Conference (A-SSCC) (December 2012).

**As Published:** <http://dx.doi.org/10.1109/IPEC.2012.6522653>

**Publisher:** Institute of Electrical and Electronics Engineers (IEEE)

**Persistent URL:** <http://hdl.handle.net/1721.1/93891>

**Version:** Author's final manuscript: final author's manuscript post peer review, without publisher's formatting or copy editing

**Terms of use:** Creative Commons Attribution-Noncommercial-Share Alike



# Ultrasonic Imaging Front-End Design for CMUT: A 3-Level 30Vpp Pulse-Shaping Pulser with Improved Efficiency and a Noise-Optimized Receiver

Kailiang Chen, Anantha P. Chandrakasan, and Charles G. Sodini  
 Department of Electrical Engineering and Computer Science  
 Massachusetts Institute of Technology  
 Cambridge, MA, USA

**Abstract**—A four-channel analog front-end (AFE) transceiver chip for medical ultrasound imaging is demonstrated. The high voltage transmitter uses a 3-level pulse-shaping technique to deliver over 50% more acoustic power for the same power dissipation, compared to traditional methods. The design requires minimum off-chip components and is scalable for more channels. The receiver is implemented with a transimpedance amplifier (TIA) topology and is optimized for noise, bandwidth and power dissipation. Based on both acoustic and electrical measurements, we demonstrate the Transmitter (Tx) efficiency improvement, Tx beamformation and the pulse-echo response, revealing the system’s full functionality.

## I. INTRODUCTION

The AFE block diagram for medical ultrasonic imaging applications is shown in Fig. 1(a). In each AFE channel, a high voltage pulser in Tx drives the ultrasound transducer to emit acoustic energy; a low noise amplifier (LNA) in receiver (Rx) amplifies echoes reflected back from the medium. Medical ultrasound systems use beamformation to improve image quality. Tx beamformation is realized by applying different delays across multiple Tx channels. Similarly, the received signals are often digitized and processed by an Rx beamformer.

Piezoelectric transducers (PZTs) are commonly used as ultrasound transducers. However, the Capacitive Micro-machined Ultrasonic Transducer (CMUT) emerges as an alternative technology for compact system integration, offering dense arrays and flip-chip bonding to electronics [1]. Interfacing to CMUTs (Fig. 1(a)) is different from PZTs because the effective load is much more capacitive and higher impedance.

For the transmitter, most power loss is associated with the capacitive load, rather than the gating and conduction loss from the power amplifier circuitry designed for a PZT load. Multi-level pulse-shaping techniques have been used for better SNR, resolution and harmonic suppression in PZT ultrasound systems [2]. Besides these benefits, this paper presents the use of multi-level technique [3] to improve the combined power efficiency of the CMUT transducer and transmitter.

For the receiver, large input capacitance limits the bandwidth and degrades noise performance. At ultrasound operating frequencies (1-20MHz), bulky off-chip inductors are needed to impedance match the source to a traditional ultrasound pre-amplifier that assumes a low-impedance source [4].

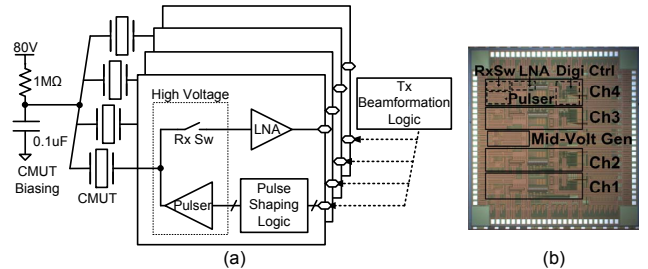


Fig. 1. (a) AFE Block diagram for medical ultrasound applications using CMUTs. (b) The four-channel AFE chip die photo.

To achieve inductor-less design, the TIA topology is used to improve the trade-off between gain, bandwidth and noise [5].

## II. TRANSMITTER DESIGN

### A. Multi-Level Pulse Waveform for Higher Efficiency

The small signal model for a CMUT element is represented by a capacitor and resistor in parallel [1]. The C is the parallel-plate capacitance between the membrane and the common node. The R is the medium’s mechanical load at the CMUT surface, transformed to the electrical port. The power dissipated by R, due to the electrical pulse’s fundamental frequency component, models the useful acoustic power delivered to the medium. The CMUT transducer used in this work is modeled as  $40pF || 80K\Omega$  per element (size  $300\mu m \times 3000\mu m$ ).

The Tx efficiency is defined as the ratio between the useful acoustic power and the total power dissipated. Resonant drivers can be used to achieve high efficiency, but off-chip inductors for each channel are once again needed due to the low operating frequencies. Alternatively, the multi-level pulse-shaping technique reduces power dissipated to charge the capacitor and increases efficiency [3]. It also requires the least off-chip components.

To show how multi-level pulse-shaping increases efficiency, assume conventional 2-level square-wave pulses (30Vpp, 3.3MHz) are used to drive a  $40pF || 80K\Omega$  load. The useful power on R at the fundamental frequency is calculated to be 2.3mW, while the dynamic power wasted on C is 119mW. An N-level waveform, using (N-1) voltage sources to charge and discharge the capacitor, reduces the wasted power to  $CV^2f/(N-1)$  while useful power decreases only slightly [3]. A 3-level pulse with 3rd order harmonic cancellation delivers

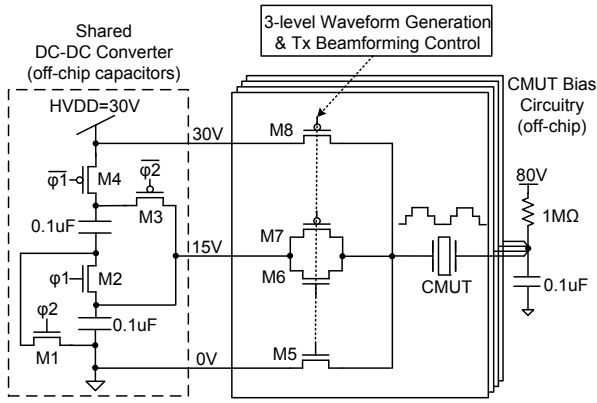


Fig. 2. Circuit schematic of the four-channel 3-level pulser with the middle-voltage generation (all transistors here are high voltage devices).

1.7mW power on R, wasting 59.5mW dynamic power. Thus, efficiency is improved considerably.

### B. 3-Level Pulser Circuit Design

The 3-level pulser is implemented on the four-channel test chip, as shown in Fig. 2. The three pulse voltage levels are 30V (HVDD), 15V and 0V (GND). The middle voltage is generated from a 2:1 parallel-series switched-capacitor DC-DC converter (M1-M4), which is shared between channels. The only off-chip components are two  $0.1\mu\text{F}$  capacitors. Because the load is much smaller than  $0.1\mu\text{F}$  (about  $0.2\text{nF}$  for four CMUT elements combined), the converter is switched at a very low frequency (10-100Hz) to save power, consuming less than 1% of the total four-channel pulsing power.

3-level pulse-shaping is implemented with four high voltage switches (M5-M8) in each channel. The relative timing differences between each channel's control signals is digitally adjustable and effectively implements the Tx beamforming. This design of multi-channel pulsers with a shared voltage converter can be extended to more voltage levels or channels.

## III. RECEIVER DESIGN

### A. LNA Optimization Methodology

Fig. 3(a) shows the small signal model of the CMUT and LNA; Fig. 3(b) plots various circuit transfer functions to help the analysis. The closed-loop TIA gain is:

$$Z_{CL} = \frac{R_f \cdot \left( \frac{1}{1+s \cdot R_f \cdot C_f} \right)}{1 + \frac{1}{F \cdot A_{OL}}}, \quad (1)$$

where  $F = Z_i / (Z_i + Z_f)$  is the feedback factor, and  $A_{OL}$  is the op-amp open-loop gain. From (1), the LNA bandwidth is determined by the smaller of the following two poles:

$$f_p = \frac{1}{2\pi R_f C_f}, \quad (2)$$

$$f_i = \sqrt{f_c \cdot f_z} = \sqrt{f_c \cdot \frac{1}{2\pi (R_f || R_i) (C_i + C_f)}}, \quad (3)$$

where  $f_i$  is the intersection between  $1/F$  and  $A_{OL}$ , which is approximately the geometric mean of  $1/F$ 's zero ( $f_z$ ) and the op-amp's unity-gain frequency ( $f_c$ ), assuming 20dB/dec roll-off. When  $f_i < f_p$ , an increase in  $R_f$  always improves LNA's gain-bandwidth product (GBP). Because DC

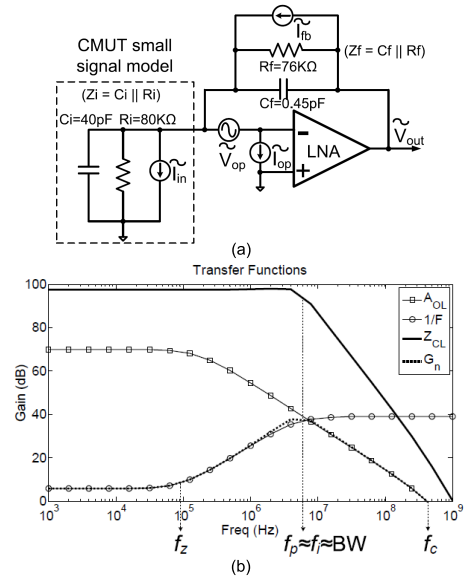


Fig. 3. (a) Small signal model and noise sources of the CMUT element and the TIA. (b) Transfer functions used for LNA optimization.

TIA Gain= $R_f$ , while bandwidth ( $=f_i$ ) is approximately proportional to  $1/\sqrt{R_f}$ . This improvement stops until  $f_i = f_p$ , at which point the LNA achieves maximum bandwidth while exploiting full op-amp GBP. The phase margin is  $45^\circ$ . Further increases in  $R_f$  no longer improve GBP because  $f_p (\propto 1/R_f)$  starts to limit the bandwidth. But phase margin continues to improve at the expense of bandwidth reduction [5].

Fig. 3(a) also shows noise sources. The noise figure is:

$$NF = 1 + \frac{R_i}{R_f} + \frac{V_{op}^2}{I_{in}^2 \cdot |Z_i| |Z_f|^2} + \frac{I_{op}^2}{I_{in}^2} + \frac{2 \cdot |V_{op} \cdot I_{op}|}{I_{in}^2 \cdot |Z_i| |Z_f|}. \quad (4)$$

From (4), a large  $R_f$  is desired to reduce its thermal noise contribution. Moreover, the noise gain ( $G_n$ ), from op-amp's input-referred voltage noise ( $V_{op}$ ) to output, has a peaking effect due to a drop in  $|Z_i|$  at higher frequencies. Both (5) and Fig. 3(b) suggest that the peaking is minimized when  $f_i = f_p$ , the same condition for maximizing the GBP and bandwidth.

$$G_n = \left| \frac{A_{OL}}{1 + F \cdot A_{OL}} \right| = \left| \frac{1}{F} A_{OL} \right| \approx \min \left( \left| \frac{1}{F} \right|, |A_{OL}| \right) \quad (5)$$

### B. LNA Implementation

The LNA optimization starts with a 5MHz bandwidth target and the optimal condition:  $f_i \approx f_p \approx BW$ .  $R_f$  is maximized while the corresponding  $C_f$ , estimated from (2), is kept larger than parasitic capacitances to maintain control over circuit stability. The op-amp unity-gain frequency is estimated from (3). Further design adjustments keep phase margin above  $60^\circ$ .

Fig. 4 shows the LNA schematic. The input stage devices (M1, M2) are biased at the boundary of strong and weak inversion for high transconductance and low noise. The Miller compensation leg (M9, Cc) keeps the op-amp second pole well beyond the closed-loop bandwidth for good phase margin. The source follower (M7, M8) lowers the op-amp output impedance for accurate feedback. To protect low voltage devices during high voltage transmissions, the high voltage

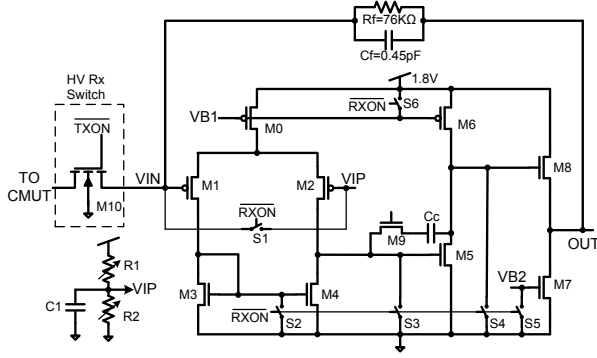


Fig. 4. The LNA schematic, implemented in the TIA topology.

Rx switch (M10) is opened and the low voltage switches (S1-S6) are closed. This also enforces the sleep mode; only the reference current remains conducting for fast wake-up.

#### IV. MEASUREMENT RESULTS

##### A. Acoustic Power Measurement

To measure Tx efficiency, the total pulsing power can be obtained electrically. However, the ultrasonic power transmitted into the medium requires acoustic measurements. From (6), acoustic power is the product of the acoustic intensity at transducer surface ( $I$ ) and the transducer surface area ( $A$ ).  $I$  is calculated from the fundamental frequency component of the RMS acoustic pressure at the transducer surface ( $p_{rms}$ ) and the acoustic impedance of the medium ( $Z_m$ ).

$$P_{acoustic} = I \cdot A = \frac{p_{rms}^2}{Z_m} \cdot A \quad (6)$$

In practice, the acoustic pressure at the transducer surface cannot be directly measured. Instead, it can be reliably back-calculated from a pressure measurement at another location. According to [6], when the transducer aperture is close to a square or circle, the pressure magnitude profile along the axial direction reaches its maximum at the boundary between the near and far field. This magnitude is roughly twice the pressure magnitude at the transducer surface.

Fig. 5(a) shows the test setup. Eight CMUT elements are connected in parallel to form an aperture of 2.4mm x 3mm, approximately a square. The solid curve in Fig. 5(b) is the corresponding acoustic simulation of the pressure field using the Field II software [7], verifying that surface pressure ( $z=0$ mm) is about half maximum pressure ( $z=5.9$ mm). Furthermore, a hydrophone (ONDA HNC0400) is used to measure the acoustic pressure magnitude along the axial axis. The result in Fig. 5(b) shows good agreement between measurement and simulation. In near field, there are deviations likely caused by the hydrophone tip distorting the pressure field. This, however, does not affect calculating the transducer surface pressure.

##### B. Tx Efficiency Measurement

Fixing the hydrophone at the near and far field boundary (5.9mm away), Tx efficiency is measured with the aforementioned method. Different pulse shapes are generated to evaluate the efficiency improvement. The pulse shape is defined by the  $\Delta/T$  ratio as shown in Fig. 6(a). When  $\Delta/T = 0$ , 2-level pulses are generated. As  $\Delta/T$  increases, the pulses turn into

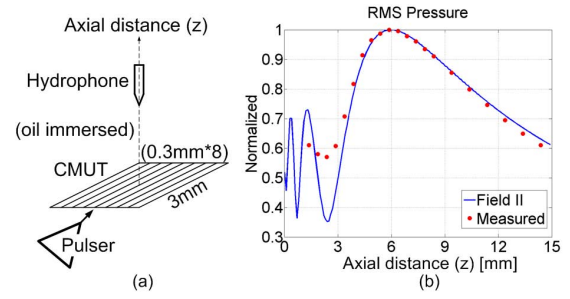


Fig. 5. (a) Acoustic power measurement setup. (b) Normalized RMS pressure along the transducer axial axis, measurement vs. simulation.

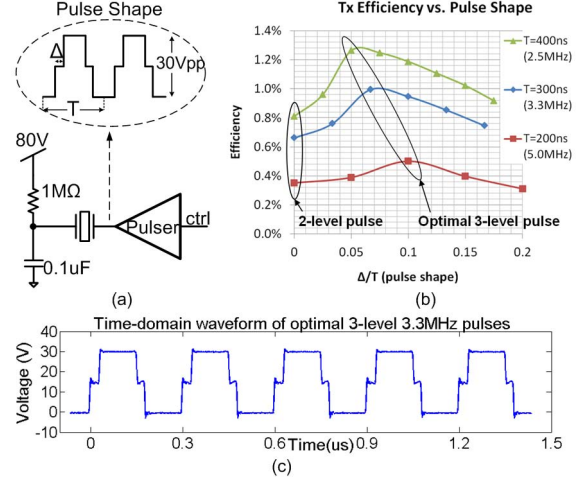


Fig. 6. (a) Tx efficiency measurement setup and pulse shape definition. (b) Measurement results using different pulse shapes. (c) Measured time-domain waveform of the optimal 3-level 3.3MHz pulses,  $\Delta=20$ ns,  $\Delta/T=0.067$

3-level, reducing the dynamic power from  $CV^2f$  to  $CV^2f/2$  and increasing the efficiency. But as  $\Delta/T$  increases further, the acoustic power starts to decrease because less energy is contained within the pulse shape. Since the dynamic power is kept at  $CV^2f/2$ , efficiency decreases. Therefore, there is an optimal pulse shape to maximize the Tx efficiency.

Fig. 6(b) shows the measurement results. Under the same total power consumption, the optimal 3-level pulser delivers 56% more acoustic power than the 2-level pulser at 2.5MHz. The relative efficiency improvements of a 3-level pulser over a traditional 2-level pulser at 3.3 and 5.0MHz pulses are 50% and 43%, respectively. Efficiency improvement is less for pulses with a shorter period, because the same RC settling transition distorts shorter pulse shape more severely, reducing useful acoustic power. Moreover, as higher frequency pulses raise dynamic power proportionally, the overall efficiency curve shifts down. HVDD value determines pulse amplitude and total power consumption, but does not have a big effect on Tx efficiency. Fig. 6(c) is a time-domain waveform of optimal 3-level 3.3MHz pulses. Table I (top part) lists optimal 30Vpp 3-level pulsing power dissipation and efficiency.

##### C. LNA Characterization

Table I also summarizes the LNA performance. The noise efficiency factor (NEF) [10] commonly used for instrumentation amplifiers is revised to compare the CMUT LNAs. The term  $V_{rms,in}/\sqrt{BW}$  is approximated by  $V_{n,in}$  (the mid-

TABLE I  
MEASURED PERFORMANCE SUMMARY AND COMPARISON

Pulser (Optimal 3-lvl)	2.5MHz	3.3MHz	5.0MHz
Power (mW)	39.4	52.4	77.6
Tx Efficiency	1.3%	1.0%	0.5%
LNA Specs			
This Work	[8]	[9]	
Target CMUT Area ( $\mu\text{m} \times \mu\text{m}$ )	300x3000	63x1037	250x250
Power [ $P_{tot}$ ] (mW)	14.3	3.81	4.0
Bandwidth (MHz)	5.2	20	10
TIA Gain ( $\text{dB}\Omega$ )	96.6	94.0	112.7
Input-referred Noise [ $V_{n,in}$ ] ( $\text{mPa}/\sqrt{\text{Hz}}$ )	0.56@3MHz	2.18@10MHz	1.8@5MHz
Noise Figure (dB) (CMUT Model)	10.3@3MHz	10.5@10MHz	N/A
Output P1dB (mVpp)	618@3MHz	84.2@8MHz	N/A
$NEF' [V_{n,in} \cdot \sqrt{P_{tot}}]$ ( $\text{mPa} \cdot \sqrt{\text{mW}/\text{Hz}}$ )	2.1	4.2	3.6
Other LNA Specs		This Work	
Sleep Power	1.5mW		
4-Ch Gain Mismatch	<0.11dB $\Omega$		
Crosstalk	<-47dBc@3MHz; <-35dBc@10MHz		
Wake-up/Sleep Time	< 1 $\mu\text{s}$		

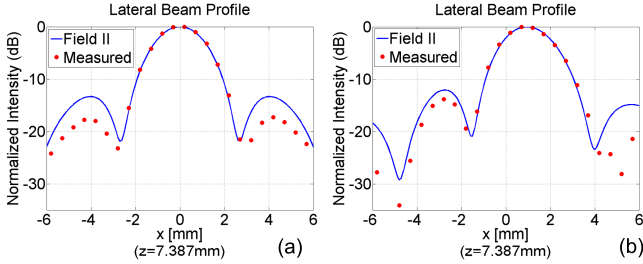


Fig. 7. (a) Measured ultrasound lateral beam profile, steered to the center (broadside). (b) Measured beam profile, 30ns delay between channels.

band pressure noise density, input-referred at the transducer surface), leading to the revised  $NEF' = V_{n,in} \cdot \sqrt{P_{tot}}$ . This work achieves better  $NEF'$  and linearity<sup>1</sup>.

#### D. Tx Beam-Steering and Pulse-Echo Measurements

Ultrasound Tx beam-steering is demonstrated by the four-channel pulsers driving four CMUT elements with 3.3MHz pulses. Fig. 7(a) and (b) shows the beam profiles in far field with 0 and 30ns delays between channels, respectively. Both measurements match Field II simulations well. In (b), the delay  $t_d$  (30ns) and the beam lateral displacement  $x$  (1.0mm) is related by:  $\frac{t_d \cdot c}{pitch} \approx \frac{x}{z}$ , where sound speed in oil  $c=1460\text{m/s}$ , CMUT element pitch=300 $\mu\text{m}$ , and depth  $z=7.387\text{mm}$ . Besides the above examples, various delay patterns for beam-focusing and steering are also measured and match simulations well.

The pulse-echo measurement tests the complete ultrasound signal chain. The pulser drives the CMUT with a wideband pulse (20ns duration, 2-level shape, shown in Fig. 8(a)). The ultrasound wave then propagates through an oil medium and reflects back at the oil-air boundary 26mm away. The echo is received by the same CMUT element and amplified by the LNA (Fig. 8(b)). The echo's FFT (Fig. 8(c)) shows the total channel characteristic, including CMUT, the oil medium

<sup>1</sup>Limited published results can be found on CMUT LNA designs, in which the CMUTs are different in size, intrinsic bandwidth and application, leading to different LNA design targets. The  $NEF'$  is used here for fair comparison.

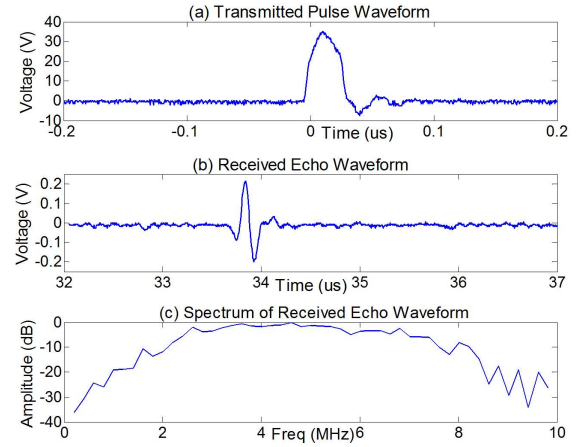


Fig. 8. The pulse-echo measurement of the complete ultrasound channel.

and LNA. It mainly reflects the band-pass characteristic of the CMUT device, with a center frequency of 4MHz and a fractional bandwidth close to 100%.

Finally, Fig. 1(b) shows a die photo of the test chip fabricated in TSMC 0.18 $\mu\text{m}$  high voltage process. Each channel occupies an area of 300 $\mu\text{m} \times 1100\mu\text{m}$ .

## V. CONCLUSION

The multi-level pulse-shaping technique is successfully applied to the CMUT transmitter for increased power efficiency. The design is highly modular and extendable to increased channels or more voltage levels. Meanwhile, the TIA topology optimizes receiver performance in the presence of a highly capacitive source. The combined electrical and acoustic measurements demonstrate complete system functionality.

## ACKNOWLEDGMENT

The authors acknowledge the support of the C2S2 Focus Center, one of six research centers funded under the Focus Center Research Program (FCRP), a Semiconductor Research Corporation entity. The authors thank Prof. Khuri-Yakub's group in Stanford University for providing CMUT devices and the TSMC University Shuttle Program for chip fabrication.

## REFERENCES

- [1] O. Oralkan, "Acoustic imaging using capacitive micromachined ultrasonic transducer arrays: devices, circuits, and systems," Ph.D. dissertation, Stanford University, 2004.
- [2] K. Kristoffersen and H. Torp, "Method and apparatus for generating a multi-level ultrasound pulse," Apr. 4 2006, uS Patent 7,022,074.
- [3] L. Svensson and J. Koller, "Driving a capacitive load without dissipating fcv2," in *1994 IEEE Low Power Electronics Symposium*.
- [4] E. Brunner, "Ultrasound system considerations and their impact on front-end components," *Analog Devices*, 2002.
- [5] Graeme, *Photodiode Amplifiers: Opamp Solutions*. McGraw Hill, 1995.
- [6] J. Bushberg, *The essential physics of medical imaging*. LWW, 2002.
- [7] J. Jensen, "Field: A program for simulating ultrasound systems," in *1996 NordicBaltic Conference on Biomedical Imaging*, 1996.
- [8] A. Nikoozadeh, "Intracardiac ultrasound imaging using capacitive micromachined ultrasonic transducer (cmut) arrays," Ph.D. dissertation, Stanford University, 2010.
- [9] I. Wygant *et al.*, "Integration of 2d cmut arrays with front-end electronics for volumetric ultrasound imaging," *Ultrasonics, Ferroelectrics and Frequency Control, IEEE Transactions on*, 2008.
- [10] M. Steyaert and W. Sansen, "A micropower low-noise monolithic instrumentation amplifier for medical purposes," *Solid-State Circuits, IEEE Journal of*, vol. 22, no. 6, pp. 1163–1168, 1987.